Robotic Needle Steering: Design, Modeling, Planning, and Image Guidance

Noah J. Cowan, Ken Goldberg, Gregory S. Chirikjian, Gabor Fichtinger, Ron Alterovitz, Kyle B. Reed, Vinutha Kallem, Wooram Park, Sarthak Misra, and Allison M. Okamura

Abstract This chapter describes how advances in needle design, modeling, planning, and image guidance make it possible to steer flexible needles from outside the body to reach specified anatomical targets not accessible using traditional needle insertion methods. Steering can be achieved using a variety of mechanisms, including tip-based steering, lateral manipulation, and applying forces to the tissue as the needle is inserted. Models of these steering mechanisms can predict needle trajectory based on steering commands, motivating new preoperative path planning algorithms. These planning algorithms can be integrated with emerging needle imaging technology to achieve intraoperative closed-loop guidance and control of steerable needles.

Noah J. Cowan · Gregory S. Chirikjian · Wooram Park · Allison M. Okamura
Johns Hopkins University, Baltimore, MD 21218, USA e-mail: ncowan@jhu.edu

Ken Goldberg
University of California, Berkeley, CA 94720, USA

Gabor Fichtinger
Queen's University, Kingston, Ontario, K7L 3N6, Canada

Ron Alterovitz
University of North Carolina, Chapel Hill, NC 27599, USA

Kyle B. Reed
University of South Florida, Tampa, FL 33620, USA

Vinutha Kallem
University of Pennsylvania, Philadelphia, PA 19104, USA

Sarthak Misra
University of Twente, 7500 AE Enschede, The Netherlands

1 Introduction

From biopsies to brachytherapy, needle-based interventions already comprise a substantial fraction of minimally invasive medical procedures. The small diameter of a needle enables it to access subsurface targets while inflicting minimal tissue damage and, once in place, the needle's lumen provides a conduit through which to deliver a wide variety of therapies, such as drugs, radioactive seeds, and thermal ablation. In addition to therapeutic delivery, needles are also commonly used for diagnostic procedures, such as biopsy. As biosensors, manipulators, ablation tools, and other "end-effector" technologies continue to get smaller, applications for needle-based interventions will also expand. This chapter reviews the state-of-the-art in steerable needle technologies, including device design, modeling, path planning, and image-guided control.

Targeting accuracy is crucial for needle-based procedures. For example, poor placement during biopses leads to false negatives. Inaccurate seed placement during brachytherapy destroys healthy instead of cancerous tissue, sometimes with catastrophic outcomes [13]. Robotic needle placement under image guidance promises to improve substantially targeting accuracy – and therefore clinical outcomes – of such procedures. Toward this end, exciting progress has been made engineering needle-placement robots for prostate biopsy and brachytherapy under a variety of imaging modalities, including ultrasound [27], magnetic resonance imaging [39, 65], and multi-imaging scenarios [48] . These robots represent a substantial advance for procedures that require multiple insertions, for example in thermal tumor ablation, because dosimetry and target planning can be updated from one insertion to the next based on intraoperative images. These general image-guided needle aiming systems work in an iterative fashion in which intraoperative imaging is used between insertions to update a plan of subsequent insertions (for example to optimize dosimetry),

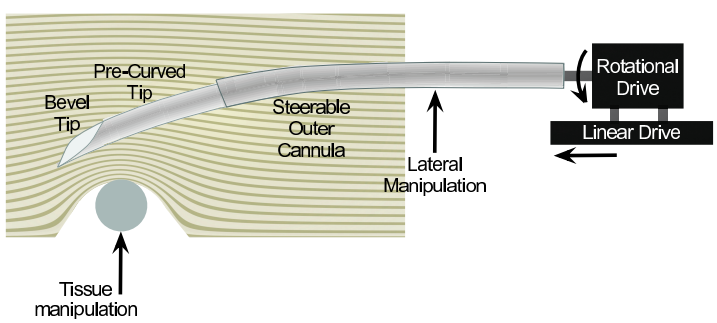

Fig. 1 This chapter focuses on subsurface needle steering, wherein a computer-integrated system can actively modify the trajectory through some combination of steering mechanisms. A needle can be steered to a target using several different methods: generating forces at the needle tip using an asymmetric tip [60, 70, 71], lateral manipulation [28], and pushing on the tissue to move the target into the needle's path [40]. A steerable cannula can be used to provide dexterity prior to (and possibly during) insertion (cf. [62] and references therein).

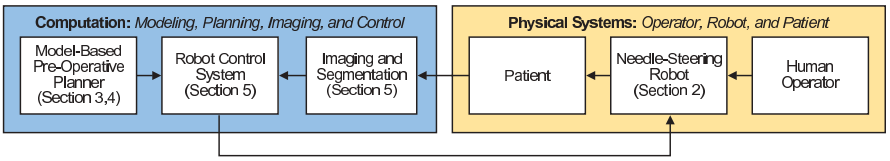

Fig. 2 A successful robotically controlled needle-steering system must be comprised of a combination of computational algorithms and physical systems.

leaving the physician in the loop to adjust the plan and/or control the invasive (insertion) degree of freedom under image feedback.

These image-guided robotic systems are clinically viable and promise to substantially enhance targeting accuracy in needle-based interventions. However, to date these systems require minimal tissue and needle deformation, and substantial effort is committed to preventing such deformation [48] because unmodeled deflections of the needle or tissue during insertion, if not compensated, will lead to gross targeting inaccuracy. Recently, needle steering researchers have begun taking the next critical step of harnessing and amplifying such deformations as mechanisms for steering a needle to a subsurface target; in this chapter we specifically focus on these recent efforts to steer needles under image feedback once they are inside the tissue using a wide variety of mechanisms, all of which involve deflecting the needle, tissue, or both as depicted in Figure 1.

This chapter describes needle steering approaches in which needles are manipulated from outside the tissue in order to change the path of the needle tip inside tissue. Alternatively, active elements could be invoked to bend the needle once inside tissue, but to our knowledge this approach has not been extensively studied from a computer-integrated surgery perspective. The advantage of passive needle steering approaches is that all the electromechanical mechanisms remain outside the patient, enabling the use of thinner needles, larger actuators, and a clearer path to clinical application.

Figure 2 shows the various computational and physical systems needed to achieve robot-assisted needle steering, and provides a graphical outline for this chapter. Section 2 provides a taxonomy of needle-steering mechanisms and robots, and Section 3 reviews the models (both phenomenological and mechanics-based) that describe these steering mechanisms. Sections 4 and 5 describe a rich variety of robotic planning, imaging, and control literature that has emerged as a consequence of these new technologies. Finally, concluding remarks are provided in Section 6.

2 Steering Approaches and Devices

This section reviews several methods for steering needles inside tissue (Figure 1), and describes example robotic devices that have been used to achieve needle steering (Figure 3). Ultimately, a combination of the needle steering approaches described

here – needle flexibility, bevel asymmetry and shape, pre-bent elements, tissue manipulation, and needle base actuation – will likely lead to systems with superior steering capability over any one method alone.

2.1 Tip-Steerable Needles

Conventional needles used in percutaneous therapy and biopsy can be classified as symmetric (e.g. conical or triangular prismatic) or asymmetric (e.g. beveled), as shown in Figure 4. It has been shown that inserting needles with asymmetric tips results in larger lateral (bending) forces than needles with symmetric tips [51]. These lateral bending forces result in deviation of the needle from a straight line path, even if the tissue does not deform. Physicians often spin asymmetric-tipped needles by hand in order to reduce needle bending during insertion, and engineers have developed devices to enhance this effect by "drilling" the needle to reduce friction and cutting forces [75]. The use of symmetric-tip needles or drilling of asymmetric-tip needles does not guarantee that a target can be reached. In both cases, needles can deviate slightly from a straight-line path due to tissue deformation or inhomogeneity, with no way to correct for this error after insertion. Also, these methods assume that there exists a straight-line path between the insertion point of the needle and the target.

In contrast, some needle steering techniques intentionally use the asymmetry of the needle tip to cause needle bending inside tissue. This can be used to enhance targeting accuracy by redirecting the path of the needle when it deviates from a desired trajectory. In addition, needle steering can allow a needle to go around obstacles or sensitive tissues to acquire targets that are inaccessible by straight-line paths. Physicians who perform targeted needle insertion currently use a number of ad-hoc methods to approximate steering, such as rotating the bevel tip of a needle, causing it to deflect slightly as inserted, or externally manipulating the tissue to guide the needle in a desired direction. However, without computer assistance, these manual needle steering techniques require the physician to have excellent 3D spatial reasoning, extensive experience, and precise coordination with high-resolution real-time image feedback.

The simplest type of asymmetric tip is a bevel tip. Bevel-tip needles are commonplace because they are straightforward to manufacture and they can be used to (slightly) direct the flow of therapeutic drugs. Bevel-tip needle steering arises from a combination of needle insertion, which causes the needle naturally to follow a curved path due to asymmetric tip forces (Figure 1), and spinning the needle about its axis, which changes the direction of subsequent bending [70]. The needle spin speed can be "duty cycled" to vary the curvature of the needle path [42], although the maximum curvature is always limited by the combined mechanical properties of the needle and tissue. In addition, "airfoil" tips can be added to increase the area of a bevel tip and increase the curvature of the needle path [26]. It is important to note that needles steered in this fashion can only steer when cutting a new path.

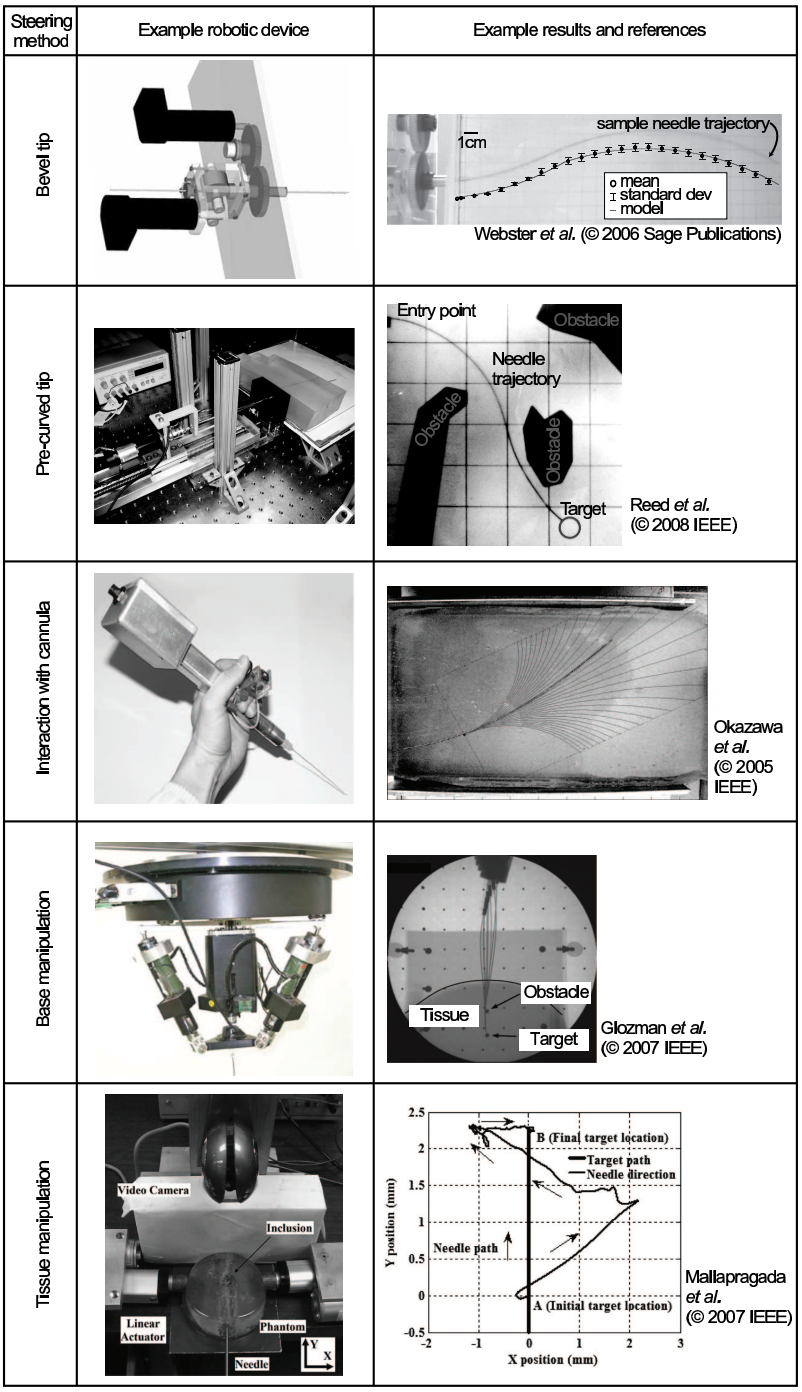

Fig. 3 Steering methods, example robotic devices, and example results from needle steering systems in the literature, including Webster *et al.* [70] [70], Reed, *et al.* [60], Okazawa, *et al.* [52], Glozman, *et al.* [28], and Mallapragada, *et al.* [40]. All figures reprinted with permission.

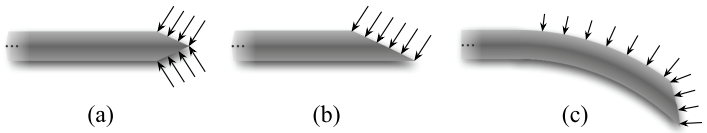

Fig. 4 Needle tips: (a) a symmetric conical tip, (b) an asymmetric bevel tip, (c) an asymmetric pre-bent/curved tip. Tip-based steering relies on an asymmetric design such as (b) or (c).

When the tissue does not deform, the entire needle will follow the tip path [71]. When a needle is removed (by simply pulling on the needle base), it follows the same path as insertion but in the opposite direction. The bevel-tip needle steering method is most effective when the needle is highly flexible (structurally having low stiffness) compared to the medium in which it is being steered. Thus, the superelastic (and biocompatible) material Nitinol has been used in some bevel-tip needle steering studies. Models for bevel-tip needle steering are discussed in Section 3.

In order to insert needles for bevel-tip steering, specialized devices are required. Automated flexible needle insertion is challenging because needles tend to buckle if not supported outside the tissue. Humans are not able to insert a needle with a precise velocity, and they may inadvertently apply lateral forces or torque about the needle axis. Webster *et al.* [71] developed two different robotic devices for steering needles using tip asymmetry. Each device is able to control insertion velocity and the rotation (spin about the needle axis) velocity. The first device is based on a friction drive concept, which has advantages of compactness and simplicity. However, major drawbacks to this design include slippage in the insertion degree of freedom (DOF), a slight spin of the needle during insertion due to imperfect alignment of the friction drive, and difficulty in measuring insertion force and spin torque. The second device involves driving the needle from its base (the distal end) while using a telescoping support sheath to prevent the needle from buckling. A needle rotation module is attached to the translational stage to spin the needle and enable steering. Although this device is larger than the first, it provides more control over needle insertion parameters, and also enables straightforward integration of force/torque sensing, making it ideal for laboratory experiments.

A needle with a curve or pre-bend near the tip achieves a smaller radius of curvature than a bevel tip alone [60, 64, 73], but can be controlled much like a bevel-tip needle [60]. The smaller radius comes from the larger asymmetry at the tip of a pre-bent needle, which creates a larger force perpendicular to the insertion direction during an insertion. Several studies have demonstrated that the radius of curvature of pre-bent [64] and curved [73] needles varies with the length and angle of the asymmetry. For long pre-curved needles, the radius of curvature approaches the radius of curvature of the needle at the tip [73]. Although using pre-bent needles allows greater dexterity, a pre-bent needle might detrimentally affect a medical procedure; for example, a pre-bent needle tip can potentially cut tissue when the needle base is rotated while not simultaneously being inserted, placing constraints on planning and control algorithms.

The curvature of a needle as it is inserted into tissue can also be modulated by changing the curvature of the needle tip. One method uses small wires inside the needle to pull the tip in the desired direction. Another method varies the tip curvature by placing a curved needle inside a stiff straight outer cannula [52]. Extending the needle so the curved section protrudes from the cannula provides an asymmetric surface that causes the needle-cannula system to bend during insertion. The amount of needle protrusion can be controlled directly and dictates the radius of curvature. For example, if the needle is entirely inside the cannula, the needle will travel in a roughly straight line. Once the cannula tip is in position, the needle can be withdrawn completely, allowing the lumen of the cannula to be used for a medical procedure. This method requires control of three DOFs: the insertion distance of both needle and cannula, and the rotation of the inner needle.

A generalization of the concentric cannula-needle system is an "active cannula" or "concentric tube" robot [24,62,63,72], in which any number of concentric flexible tubes can interact with each other to change the three-dimensional (3D) shape of the device. Rotating and inserting/retracting each of the individual tubes allows control of the device tip within a large set of configurations. These concentric-tube devices do not depend directly on needle-tissue interaction, but can be used as steerable needles.

2.2 Lateral Manipulation

An alternative method of steering the needle involves moving the base of the needle perpendicular to the insertion axis [19, 28]. The perpendicular motions cause the entire needle shaft to move inside the tissue where the needle acts, much like a beam resting on a compliant fulcrum. Once the needle is inserted sufficiently far inside the tissue, motion of the needle base orthogonal to needle shaft direction causes the tip to move in roughly the opposite direction. However, there is substantial path dependence, making it challenging to develop closed-form models (Section 3.4).

Maneuvering a needle using lateral manipulation may require Cartesian motions and rotations. The only DOF not required is the rotation of the needle around the insertion axis, which is one of the two required inputs to control a tip-steered needle, so lateral manipulation may allow added maneuverability to a tip-steered needle.

Lateral manipulation can achieve large changes in the needle path near the surface, but the effect decreases as the needle is inserted further into the tissue. The needle must transmit all the force from the base to the tip and, as the needle is inserted further, more tissue can resist the force and the moment arm increases. To generate the same change in path throughout the insertion, the force at the base must increase, but the tissue can only withstand so much force before tearing. Tip-steered needles, however, are approximately depth independent, since the dominant steering force is generated at the tip of the needle. Lateral manipulation and tip-steered needles can be used together for additional control over the needle throughout the entire insertion.

2.3 Tissue Manipulation

In addition to manipulating the needle in order to acquire targets in soft tissue, it is also possible to manipulate the *tissue* in order to move targets into the path of the needle or push obstacles and sensitive tissues out of the path of the needle. Physicians already perform such tissue manipulation by hand, and recent work has provided insight regarding robotic control to achieve the same effects. Robotic tissue manipulation systems could improve both the accuracy of target acquisition and the accessibility of targets, and be combined with the other needle steering approaches described above.

Mallapragada *et al.* [40] developed a method for real-time tumor manipulation, in which a robotic controller takes as input real-time medical images of a tumor and outputs an appropriate external force to move the tumor to a desired position. During needle insertion (in an approximately straight line path), blunt robotic end-effectors push on the tissue to move the tumor onto the needle path (Figure 3). In simulations, Torabi *et al.* [67] considered a more complex tissue manipulation problem, in which robots are used to both move obstacles out of the way of the path of the needle and the target onto the path of the tissue. A two-dimensional mass-spring simulation demonstrated the effectiveness of the planner/controller combination in reducing targeting errors and shifting obstacles.

3 Modeling

The design of needle steering planners and most types of controllers requires a model of needle-tissue interaction that predicts needle or needle-tip motions given inputs at the needle base. This section describes several phenomenological models that capture needle-tissue behavior sufficient to inform planning and control design, as well as ongoing efforts to create more accurate mechanics-based models.

3.1 Nonholonomic Steering

A bevel-tip needle inserted into homogenous tissue will follow a stereotyped path. Webster *et al.* [70] demonstrated that the kinematics of a bevel tip needle can be modeled as a non-holonomic system with a constant steering constraint. According to this model, the needle tip advances forward in a curved path, but cannot translate when embedded in tissue. The kinematic model is similar to the motion of a unicycle or bicycle with the handlebars locked in one position. The wheels of a bicycle cannot instantaneously move sideways, yet the bicycle can attain any desired pose in the plane through a more complex sequence of motions. Whereas bicycle steering occurs in plane, needle steering occurs in 3D space.

Webster *et al.* performed experiments and statistical analysis verifying that the nonholonomic model fits a limited battery of insertions and found that the two-parameter bicycle model described the needle behavior better than a single-parameter unicycle model, although the unicycle model's simplicity and reasonable accuracy has made it a good choice for control systems design [35–38]. Many of the models, planning algorithms, and control systems described throughout the remainder of this chapter build upon these nonholonomic models of needle motion.

The kinematic model can be mathematically expressed as follows. Attach a reference frame to the needle tip with the local z-axis denoting the tangent to the needle shaft and x-axis denoting the axis orthogonal to the direction of infinitesimal motion induced by the bevel (i.e. the needle bends in the instantaneous y-z plane). The nonholonomic kinematic model for the evolution of the frame at the needle tip was developed based on a unicycle model in [54, 70] as

$$\xi(t) = \left(g^{-1}(t)\dot{g}(t)\right)^{\vee} = \left[\, \kappa v(t) \;\, 0 \;\, \omega(t) \;\, 0 \;\, 0 \;\, v(t) \,\right]^{T}, \tag{1}$$

where $g(t)$ is the element of the Euclidean motion group, $\mathrm{SE}(3)$ and ξ is the element of $\mathrm{se}(3)$, which is the Lie algebra associated with $\mathrm{SE}(3)$. Here, $g(t)$ is the 6-DOF pose of the frame attached to the needle tip in 3D space and $\xi(t) \in \mathbb{R}^6$ in denotes the 6D translational and rotational velocity of the frame. The control inputs, $\omega(t)$ and $v(t)$, are the rotation and insertion velocities, respectively, and κ is the curvature of the needle curve. The frames and parameters for the needle are shown in Figure 5.

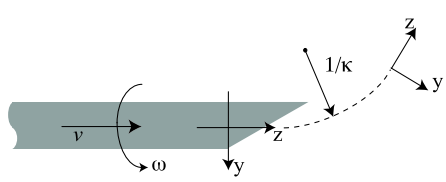

Fig. 5 The definition of parameters and frames in the nonholonomic needle model [54, 70] (Reprinted with permission from [56], © 2010 Sage Publications).

3.2 Stochastic Modeling

Although the kinematic model for needle steering describes the motion of the needle, there is inherently variation between insertions. If everything were certain, and if this model were exact, the motion, $g(t)$, could be obtained by simply integrating the ordinary differential equation in (1). However, a needle that is repeatedly inserted into a medium, such as a gelatin used to simulate tissue [70], will demonstrate an ensemble of slightly different trajectories.

A simple stochastic model [54, 55] is obtained by adding noise to the two input parameters in the ideal model:

$$\omega(t) = \omega_0(t) + \lambda_1 w_1(t) \quad \text{and} \quad v(t) = v_0(t) + \lambda_2 w_2(t),$$

where $\omega_0(t)$ and $v_0(t)$ are what the inputs would be in the ideal case, $w_1(t)$ and $w_2(t)$ are uncorrelated unit Gaussian white noises, and λ_1 and λ_2 are constants. Thus, the nonholonomic needle model with noise is

$$\left(g^{-1}(t)\dot{g}(t)\right)^{\vee} dt = \begin{bmatrix} \kappa v_0(t) & 0 & \omega_0(t) & 0 & 0 & v_0(t) \end{bmatrix}^T dt + \begin{bmatrix} 0 & 0 & \lambda_1 & 0 & 0 & 0 \\ \kappa\lambda_2 & 0 & 0 & 0 & 0 & \lambda_2 \end{bmatrix}^T \begin{bmatrix} dW_1 \\ dW_2 \end{bmatrix},$$

where $dW_i = W_i(t+dt) - W_i(t) = w_i(t)dt$ are the non-differentiable increments of a Wiener process $W_i(t)$. This noise model is a stochastic differential equation (SDE) on $\mathrm{SE}(3)$. As shorthand, we write this as

$$(g^{-1}(t)\dot{g}(t))^{\vee} dt = \mathbf{h}(t)dt + H d\mathbf{W}(t).$$

3.3 Torsional Modeling

In order to change the direction of curvature of a tip-steered needle, the base of the needle must be rotated. As the needle rotates inside the tissue, friction opposes the needle's rotation and can cause the angle at the tip to lag behind the angle at the base (Figure 6). Some artificial tissues exert enough friction to cause over a 30° difference between the base and tip angles for an insertion distance of 10 cm [61]. These large angle misalignments are thought to account for some of the reduced performance in the image-guided controllers discussed in Section 5.3. Although the torques applied during a prostrate brachytherapy are not significant enough to cause any torsion windup in the typical steel needles used for percutaneous procedures [58], the torques are likely to cause a significant discrepancy in the flexible needles required for needle steering [61]. Unfortunately, there is a tradeoff that arises due to the flexibility of the needle; increased flexibility enhances steering, but also increases the amount of torsion windup when rotating the needle.

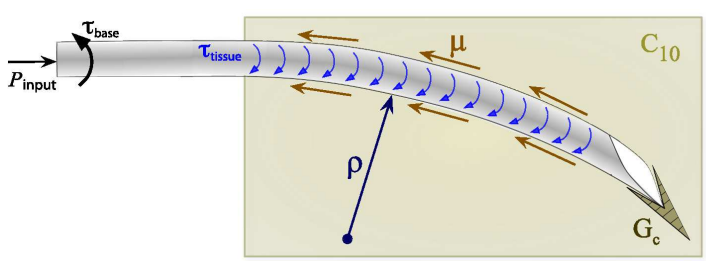

Fig. 6 Schematic of a bevel-tip needle interacting with a soft elastic medium: Models have incorporated tip forces generated by rupture, tissue properties (toughness: G_C, nonlinear elasticity: C_{10}), needle properties (bevel angle: α and flexural rigidity: EI), and the torque generated from the needle-tissue interaction when the needle is rotated.

State-of-the-art imaging is unable to accurately measure the tip angle of the small needles used in percutaneous procedures, but the angle lag at the tip of the needle can be estimated using a force sensor at the base of a bevel-tip needle [1, 59]. One method to overcome torsion estimates the angle lag from the measured torque and rotates the needle several times in alternating directions to orient the entire needle shaft to the desired orientation [59]. However, this method only works when the needle is not being inserted during rotation.

When the needle is being simultaneously rotated and inserted through the tissue, the effects of stiction are not present since the needle is continuously sliding past the tissue. In this case, the needle-tissue interaction can be modeled as viscous damping and a modal analysis can determine the dynamics of the needle tip, and a parsimoneous finite-dimensional model can be obtained using modal analysis [61]. The estimated tip position and measured base angle can then be used in a controller to increase the base-tip convergence time and decrease the positioning error.

3.4 "Tissue Jacobian" Approaches

Changing the insertion direction of a needle by manipulating the base of the needle outside the tissue requires an understanding of how the flexible needle will interact with soft tissue. Two models relate the motions at the base of the needle to motions at the tip of the needle. In one method, the inverse kinematics of the needle are used to determine the path [28]. The kinematics are derived from modeling the soft tissue as springs with stiffness coefficients that vary along the length of the needle. The needle is modeled as a linear beam.

Another model involves numerically calculating the Jacobian for the tissue deformation and needle deflection [19]. Given the velocity of the base, this model determines the tip velocities. A needle path is computed based on potential fields: a repulsive field drives the needle away from obstacles and an attractor field drives the needle toward the desired target.

3.5 Toward Fundamental Mechanics-Based Models

Several research groups have developed physics-based needle and soft tissue interaction models [7, 16, 18, 31, 32, 49]. A general survey of surgical tool and tissue interaction models, which describes both physics- and non-physics-based interaction models, is provided in [43]. As described in Section 3.1, Webster *et al.* [70] presented a phenomenological nonholonomic model for steering flexible needles with bevel tips. The parameters for their model were fit using experimental data, but this model is not informed by the fundamental mechanical interaction of a needle with an elastic medium. For improved planning and control, as well as the optimization of needle design for particular medical applications, an ideal model would

relate needle tip forces to the amount of needle deflection based on the fundamental principles of continuum and fracture mechanics.

Mechanics-based needle-tissue interaction models aim to relate the needle's radius of curvature to the material and geometric properties of the tissue and needle. The radius of curvature of a bevel-tipped needle is a function of several parameters (Figure 6): the needle's Young's modulus (E), second moment of inertia (I), and bevel-tip angle (α); the tissue's nonlinear (hyperelastic) material property (C_{10}), rupture toughness (G_c), and coefficient of friction (μ); and the input insertion force from the robot controller $\left(P_{\text{input}}\right)$.

Misra *et al.* [44] investigated the sensitivity of the tip forces to the tissue rupture toughness, linear and nonlinear tissue elasticity, and needle bevel-tip angle. In order to find the forces acting at the needle tip, they measured the rupture toughness and nonlinear material elasticity parameters of several soft tissue simulant gels and chicken tissue. These physical parameters were incorporated into a finite element model that included both contact and cohesive zone models to simulate tissue cleavage. The model showed that the tip forces were sensitive to the rupture toughness.

In addition, Misra *et al.* [45–47] developed an energy-based formulation incorporating tissue-specific parameters such as rupture toughness, nonlinear material elasticity, interaction stiffness, and needle geometric and material properties. This mechanics-based model was guided by microscopic and macroscopic experiments. The functional form for the deflection of the needle in an elastic medium was initially assumed and the Rayleigh-Ritz approach was used to evaluate the coefficients of the deflection equation. The Rayleigh-Ritz method is a variational method in which the minimum of a potential defined by the sum of the total energy and work done by the system are calculated. The system potential, Λ, of a needle interacting with an elastic medium, is given by

$$\Lambda = \underbrace{(N_E + S_E)}_{\text{energy}} + \underbrace{(-W_Q - W_P - W_R)}_{\text{work}} + \underbrace{P_{\text{input}} l_i}_{\text{input work}}, \tag{2}$$

where N_E and S_E are the energies associated with needle bending and needle-tissue interaction, respectively, and W_Q and W_P are the work due to transverse and axial bevel tip loads, respectively, and W_R is the work done to rupture the tissue. Explicit expressions for each of the terms in (2) are provided in [46]. Simulation results follow similar trends (deflection and radius of curvature) to those observed in experimental studies of a robot-driven needle interacting with different kinds of gels. These results contribute to a mechanics-based model of robotic needle steering, extending previous work on kinematic models.

4 Needle Path and Motion Planning

Directing steerable needles to specific targets while avoiding anatomical obstacles requires planning paths through the patient's anatomy. For steerable needles, this planning is often beyond the capabilities of human intuition due to the complex kinematics discussed in Section 3 and the effects of tissue deformation, tissue inhomogeneities, and other causes of motion uncertainty. In order to harness the full potential of steerable needles, efficient computational methods can help physicians plan paths and actions.

When steerable needles are used with image guidance, the physician can specify the target to be reached, feasible needle insertion locations, and the locations of anatomical obstacles, including those that cannot be passed through such as bones as well as sensitive anatomical structures that ought to be avoided such as blood vessels or nerves. Using patient-specific information about such anatomical structures, a motion planning algorithm determines a sequence of actions (such as insertions and bevel direction changes for bevel-tip needles) so that the needle tip reaches the specified target while avoiding the clinician-specified obstacles. Planning can be used purely preoperatively to generate a plan that is then followed by the robot or physician during the procedure. Planning can be also used intraoperatively by updating the plan in real time based on intraoperative images and other sensor feedback.

4.1 3D Path Planning with Obstacles

Motion planning algorithms have been developed to compute optimal trajectories for bevel-tip steerable needles in 3D environments with obstacles. Using the model of Webster *et al.* [70], Duindam *et al.* [22] computed piece-wise helical motions of the needle tip. The method optimizes a cost function that numerically quantifies the planning objective, including penalties for deviation from the target location, large control actions, and obstacle penetration. The algorithm uses a suitable discretization of the control space to quickly compute a needle path with (locally) minimal cost. In a second algorithm, Duindam *et al.* rely on an explicit expression of the inverse kinematics of the needle to generate a range of valid needle paths from start to target, from which the best solution can be selected [23]. Although this algorithm generally does not compute a (locally) optimal solution, it does not require iteration to converge to a solution and is hence much faster than the first algorithm. Depending on the required balance between speed and optimality, either algorithm can be advantageous. Xu *et al.* present a sampling-based motion planning technique based on the Rapidly-exploring Random Trees (RRTs) method [74]. The planner quickly builds a tree to search the configuration space using random sampling of the control space. Recently, Hauser *et al.* explored the use of a model predictive control strategy that chooses a needle twist rate such that the predicted helical trajectory minimizes the distance to the target, which can be used both for preoperative planning and intraoperative control [30].

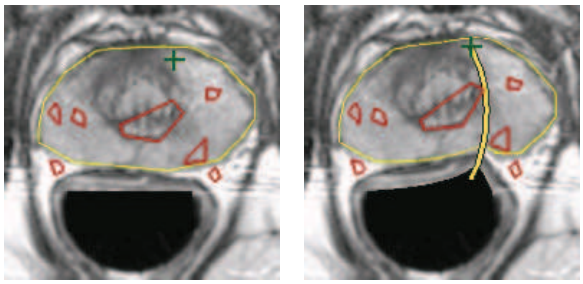

(a) (b)

Fig. 7 A needle steering planner that considers 2D tissue deformation [6] (© 2005 IEEE), reprinted with permission. The magnetic resonance images show a tumor target (cross) in the prostate with obstacles that preclude a straight-line trajectory. The images show (a) the initial configuration and (b) a planned path for a bevel-tip steerable needle deployed from a transrectal probe. This locally optimal plan compensates for tissue deformations, avoids obstacles, and minimizes insertion distance.

4.2 Planning for Deformable Tissues

Inserting needles into soft tissues causes the surrounding tissues to displace and deform. Ignoring these deformations can result in substantial placement error. For example, while performing prostate brachytherapy cancer treatment, an experienced physician implanting radioactive seeds in 20 patients achieved an average placement error of 0.63 cm, a substantial error of over 15% of average prostate diameter [66].

Computer simulations that model soft tissue deformations can assist in preoperative planning by enabling clinicians a priori to optimize paths for needle insertion procedures [5]. Building on their prior work on simulation of rigid needles into deformable tissue [8,10,11], Alterovitz *et al.* developed a simulation of bevel-tip steerable needles in 2D [6] and Chentanez *et al.* developed a 3D simulation [14]. These simulations model the coupling between a steerable needle and deformable tissue using the finite element method (FEM) – a mathematical method based on continuum mechanics for modeling the deformations and motions of solids and fluids. The simulations model patient-specific anatomy using a mesh composed of triangular (2D) or tetrahedral (3D) elements. As the needle moves, the simulations model needle friction and cutting forces, as described in the models in Section 3. The simulations use novel re-meshing to ensure conformity of the mesh to the curvilinear needle path. Achieving a computationally efficient simulation is challenging; the FEM computation in [14] is parallelized over multiple cores of an 8-core 3.0 GHz PC and achieve a 25 Hz frame rate for a prostate mesh composed of 13,375 tetrahedra.

To help physicians anticipate and correct for the effects of tissue deformations, Alterovitz *et al.* developed a planner for bevel tip steerable needles that uses the simulation to compensate for predicted tissue deformations and to minimize placement error [6]. To compute the optimal initial insertion location and orientation, the planner formulates the planning problem as an optimization problem. The planner

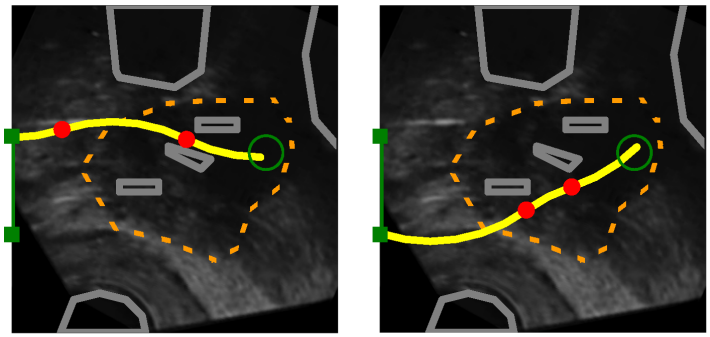

(a) Shortest path (b) Maximizing probability of success

Fig. 8 The motion planner computes a sequence of insertions (curved lines) and direction changes (dots) to steer the needle from a start region at the left to the target (circle) while avoiding obstacles (grey outlines) [4] (© 2008 Sage Publication), reprinted with permission. The planner computes (a) the shortest path, which passes close to obstacles, and (b) a better path generated by explicitly considering uncertainty in the planning stage, which increases the probability of successfully avoiding obstacles while reaching the target.

minimizes the distance the needle is inserted subject to the constraints that the needle tip reaches the target, the needle path does not intersect any obstacles, and the control inputs are within feasible ranges. The planner uses the simulation to predict the path of the needle when evaluating the objective function and constraints, and it employs a penalty method to convert the nonlinear, constrained optimization problem into a sequence of unconstrained problems that can be solved quickly. The method computes a solution in just a couple of minutes on a standard processor.

As discussed in Section 2, some needle steering approaches leverage tissue deformation in order to generate curved paths through tissue. DiMaio and Salcudean introduced simulation and planning for flexible symmetric-tip needles in 2D deformable tissue by controlling motion of the needle base [19]. Their Jacobian-based planner relied on a quasi-static FEM simulation to estimate the needle and tissue deformations. This simulation was designed for offline planning and does not achieve frame rates needed for interactive simulation or global optimization. Glozman and Shoham accelerate this approach by approximating the tissue using springs to compute local, but not global, deformations, enabling a fast planning algorithm based on inverse kinematics [28].

4.3 Planning under Motion Uncertainty

Although detailed models are available for predicting the motion of steerable needles, a steerable needle may deflect from its expected path due to tissue inhomogeneities, transitions between tissue layers, local tissue deformations, patient variability, and uncertainty in needle/tissue parameters. Medical imaging can be used

to measure the needle's current position and orientation, but this measurement by itself provides no information about the effect of future deflections on procedure outcome.

Alterovitz *et al.* have developed planners that explicitly consider uncertainty in needle motion in order to maximize the probability of avoiding collisions and successfully reaching the target [3, 4, 12]. The Stochastic Motion Roadmap (SMR) framework efficiently samples the state space, builds a "roadmap" through the tissues that encodes the system's motion uncertainty, formulates the planning problem as a Markov Decision Process (MDP), and determines a solution using dynamic programming to maximize the probability of successfully reaching the target. This framework was applied to compute steerable needle paths around obstacles to targets in tissues imaged using 2D slices. Explicitly accounting for uncertainty can lead to significantly different motion plans compared to traditional shortest paths, such as longer paths with greater clearance from obstacles in order to increase the probability of success.

Reed *et al.* integrated this planner into an image-guided robotic needle steering system that includes a robotic device that can control the needle in artificial tissue and a low-level image-guided feedback controller to maintain the needle on a 2D plane [59]. The needle successfully reached targets in artificial tissues and the system experimentally demonstrated that the planner is robust to initial positioning errors of 2 cm.

The SMR framework described above transforms the continuous workspace into a discrete roadmap that encodes actions, motions, and uncertainty. An alternative approach considers the ensemble of needle trajectories obtained by repeated insertion with the same control inputs. The trajectories will be slightly different from each other due to uncertainty that may exist in the control mechanism and the interaction between the needle and the tissue. Park *et al.* [54, 55] developed such a path planning method for needle steering that actively utilizes this stochastic behavior of the flexible needles. This algorithm is an adapted version of the path-of-probability (POP) algorithm in [25]. A similar trajectory planning method can also be found in [41].

In the POP algorithm, the whole trajectory is obtained by serially pasting together several intermediate paths. Based on the stochastic behavior of the flexible needle, the probability density function of the needle tip pose can be estimated and evaluated. The intermediate steps are determined so as to maximize the probability that the needle tip hits the target pose.

Figure 9 shows the concept of the POP algorithm. The planning goal is to find a needle path that starts at $g_0 \in SE(3)$ and ends at $g_{goal} \in SE(3)$ using M intermediate steps. The homogeneous transformation matrix, $g_i \in SE(3)$ $(i = 1, 2, ..., M)$, represents the position and rotation of the ith frame with respect to $(i-1)^{th}$ frame. Suppose that the $(i-1)$ intermediate steps $(g_1, g_2, \cdots, g_{i-1} \in SE(3))$ have already been determined. The intermediate step, g_i, is determined to maximize the probability that the remaining needle insertion reaches the goal. The shaded ellipses depict the probability density function that represents the probability of the needle tip pose after the remaining $(M-i)$ steps. In other words, after the remaining $(M-i)$ steps,

the final pose will be placed in the dark area with higher probability than the bright area. Comparing the two simplified cases in Figure 9, if the previous intermediate steps $(g_1, g_2, \cdots, g_{i-1})$ are the same for both cases, g_i shown in Figure 9(b) is a better choice, because it guarantees with higher probability that the final pose reaches the goal pose.

Computing the probability density function plays a crucial role in the POP algorithm. The probability density function can be obtained using the stochastic model for the flexible needle stochastic differential equations (SDE) as reviewed in Section 3.2. The Fokker-Planck equation corresponding to the SDE defines a function representing the probability density of the needle tip pose. Rapid evaluation of the probability function is required for fast path planning. Specifically, the probability density is estimated by a Gaussian function [55, 57], and the mean and covariance are estimated using error propagation techniques developed for the motion groups [68, 69].

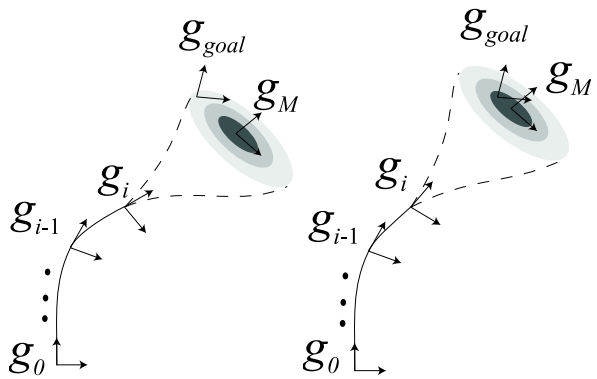

Fig. 9 The path-of-probability algorithm at the *i*th step [56] (© 2010 Sage Publications), reprinted with permission. (a) An intermediate step, g_i, resulting in low probability of reaching the goal. (b) An intermediate step, g_i, resulting in high probability of reaching the goal.

5 Image Guidance

5.1 Needle Localization in Medical Images

The problem of needle localization in images might seem straightforward, yet practical implementations have seldom appeared. Usually, a cascade of basic image filters (such as thresholding, edge detection, image smoothing and noise removal filters) are combined with more sophisticated feature detections routines, such as a variant of Hough transform. Significant literature exists on the theory, use, and extension of Hough transform; a succinct summary and background reading are given

in [20]. Many localization methods entail two steps: first, points or fragments of the needle are extracted from the images and then a 3D geometric model (straight line, polynomial, etc.) is fit to the fragments, typically in a least-squares optimization scheme. The two steps can be combined in a probabilistic framework, where points of high probability of belonging to the needle are fitted on a 3D geometrical model. This approach is especially suitable when the quality of images (resolution, dynamic range, etc.) is poor, such as in ultrasound images. In this section, we survey the most popular needle localization methods used with various imaging modalities, namely fluoroscopy, computed tomography (CT), magnetic resonance imaging (MRI), and ultrasound (US).

Fluoroscopy. Metal needles, being of high density, tend to be visible in X-ray images such as those obtained from CT and fluoroscopy. In fluoroscopy, a single projection image is insufficient for reconstruction of the needle in 3D. Two images are sufficient to reconstruct a straight needle, while three or more images and some amount of prior knowledge about the curve are necessary for 3D reconstruction of a curved needle. For needles that lie in a plane, polynomial models are preferable because polynomials are invariant to perspective projection. For example, Jain *et al.* used a combination of 0th-, 1st-, and 2nd-degree polynomials to fit image points on a 3D model with sub-millimeter and sub-degree accuracy [33]. When a needle is driven out of plane, spatial reconstruction becomes more demanding and requires more images and/or a more elaborate 3D model for the needle. A seemingly innocuous and often underrated problem in fluoroscopy is that the device must be precisely calibrated, including the relative pose of the fluoroscopy images [33].

CT. Although CT can produce a 3D volume, needle insertion is often performed in a single 2D plane, with the CT gantry tilted in order to show the needle in the 2D image. Newer CT scanners provide short acquisition time with reasonably low dose, convenient for intermittent observation of the needle. Many CT scanners also provide continuous beam mode, yielding a single CT image of low resolution at high frame rate ($\approx$10 fps). There is a trade-off between image quality (resolution and dynamic range), frame rate, and X-ray dose. Modern CT scanners can also produce multiple slices (i.e. thin 3D volume) and high-end scanners even provide multiple slices in continuous beam mode.

A universal problem of any X-ray imaging modality (fluoroscopy and CT included) is that for safety reasons image acquisition cannot be triggered by the surgical navigation software and images are acquired under the command of a human operator. This process is time consuming, cumbersome and error prone. The available alternative is using continuous X-ray, exposing the patient and physician to excessive radiation.

MRI. For needle localization, the one major advantage of MRI over X-ray imaging is the absence of harmful radiation. In practice, there is typically a compromise on both spatial resolution and acquisition time: MR images used in surgical guidance tend to be of much lower resolution than diagnostic images, and the acquisition is usually not real-time. A further disadvantage of MRI is that metal needles create a large signal void in the image. Further, the signal void does not coincide with the true position of the needle, and the displacement between the two depends on the

configuration of the needle, the B0 field and the gradient field [17]. It is not uncommon for a 1 mm diameter needle to leave a 5 mm signal void in the image; hiding both the needle and the surrounding anatomy.

Ultrasound. Ultrasound (US) is an attractive needle guidance modality, due to its low cost, widespread availability, and safety. US imaging is an operator-dependent manual process. It also causes some degree of tissue deformation and dislocation as the transducer makes contact with the tissue scanned. US images tend to be noisy, due to reflections, reverberations, shadows, air pockets, and biological speckle, which makes needle localization challenging. Some needle localization methods use 2D images [15, 20, 53], while others compound a 3D volume from a tracked sweep of 2D images [2, 21]. For completeness, we note that, due to current limitations on voxel resolution and transfer speed, 3D US probes have not been practical for image-based needle guidance. Novotni *et al.* tracked laparascopy instruments (which are larger than needles), but this requires a research agreement with the vendor of the ultrasound machine [50].

To localize straight needles in 2D ultrasound, Ding *et al.* introduced a sophisticated derivative of the Hough transform [20]. Cheung *et al.* proposed an enhancement algorithm that maximizes the received reflections by steering the ultrasound beam to be precisely perpendicular to the needle [15]. Surface-coated needles are available commercially, to enhance ultrasonic visibility of the needle, which in turn increases friction during insertion and thus may not be appropriate for needle steering. Okazawa *et al.* localized bent needles in a 2D image plane by warping an initial guess straight line into a 2D parametric curve fitting on probable needle points [53]. This method works well for conventional needles, but it breaks under excessive curvature often observed with elastic needles and catheters. Ding *et al.* constructed a 3D volume from a sweep of tracked 2D images, cropped the volume sensibly and created several orthogonal projection images. They segmented the needle in the projections with the Hough transform and then reconstructed the needle from its 2D projections as a straight line. Aboofazeli *et al.* recently localized curved non-planar needles in 3D space [2]. They pre-filtered a compounded 3D US volume and produced series of 2D images by ray casting. In the projected images, the needle was segmented with the Hough transform and fitted onto a polynomial model. From the series of 2D polynomial curves, they reconstructed a surface that contains the needle. This 3D surface was smoothed and the needle was detected on the surface using the Hough transform followed by a polynomial curve fitting. The end result was a continuous 3D curve consisting of polynomial patches.

Localization of the needle tip has been a major challenge, especially in 2D US, where it is difficult to determine whether the needle tip is inside or outside the plane of imaging. The non-uniform thickness of the US beam adds further to the localization error. When using bevel-tip needles, the physician often rotates the needle to create a visible, fluctuating artifact at the needle tip. Harmat *et al.* created mechanical vibrations on the needle tip and measured the resulting Doppler effects [29]. Their prototype robustly detected the needle tip, but it did not seem to provide sufficient accuracy for localizing the needle tip for controlled insertion.

5.2 State Estimation of Unmeasured Degrees of Freedom

As described above, except in MR images, researchers have had reasonable success in localizing needles, but estimating the full 6-DOF pose of the needle tip directly from medical images, including rotation about the needle axis, remains elusive. However, this rotation information is necessary for control and planning purposes. To overcome this, Kallem *et al*. designed dynamical observers (analogous to a Kalman filter) based on kinematic models of needle steering that can be used to estimate full 6-DOF needle tip pose from a sequence of 3D position measurements [34]. They showed that the rotation of the needle tip may be inferred from the measurements of the needle tip position over time and developed model-based asymptotic observers that exploit the task-induced reduction to estimate the full needle pose.

Needle steering is highly nonlinear, which makes the estimation and control problem coupled, unlike in linear systems. Building on the nonholonomic model of Webster *et al.* (see Section 3.1), Kallem and Cowan [37, 38] exploit the fact that, to drive the needle to a desired 2D plane (y-z plane without any loss of generality), only three of the six degrees of freedom need to be considered. Using this reduction, they first developed an observer to estimate the x position, the pitch of the needle tip, and the roll of the needle from just x position measurements. In [34] a linear model to represent the dynamics of the other three states (y, z positions and yaw of the needle) is created by state immersion into a finite higher dimensional manifold; based on this, Luenberger observers for this smaller system are designed. This two-stage coupled observer estimates the complete needle orientation and also filtered the noisy position measurements. For other tasks, similar controller-observer pairs need to be developed to estimate needle orientation.

5.3 Image-Guided Control of Needle Steering

As described in Section 3, considerable progress has been made developing "plant models" for manipulating a needle from outside the patient. These models enable development of model-based feedback controllers to steer the needle inside the tissue. Glozman and Shoham [28] developed an image-guidance strategy for flexible needles without a bevel tip. First they plan a needle path that avoids obstacles in the workspace. Then at every time step they invert a virtual spring model to obtain the translation and orientation of the needle base (the inputs) in order to drive the needle back to the planned path in one step.

Kallem and Cowan [37, 38] took a systems-theoretic perspective to develop feedback-based controller-observer pairs for tip-steerable needles. A tip-steerable needle has been modeled as a 6-DOF nonholonomic system (1) with two inputs and nonholonomy degree four. Furthermore, when the needle is pulled out of the tissue, no cutting forces are generated and thus the needle follows the same path as during insertion into the tissue. These constraints imply that asymptotic controllers do

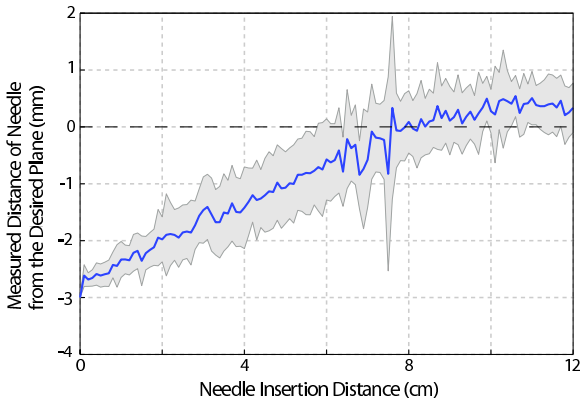

Fig. 10 Nine experimental trials were used to validate an image-guided controller [38] (© 2009 IEEE), reprinted with permission. The mean distance of the needle-tip from the desired plane of all trials is plotted against the insertion distance of the needle into the tissue (solid blue line; gray region indicates mean ± standard deviation). All trials control approach the desired 2D plane and stay within the noise levels of the position measurements of approximately 1 mm.

not exist for certain tasks, such as driving the needle tip to reach a desired pose in 6 DOF or following a circular path whose radius is the natural radius of curvature of the needle inside the tissue. To overcome these challenges, the approach taken in [37, 38] is to develop low-level, asymptotic controllers that only control a subset of the degrees of freedom. These controllers are designed to cooperate with the higher-level 2D planners from Alterovitz *et al.* [9, 12]. These planners, which rely on the needle staying within a specified 2D plane, construct a sequence of circular arcs of the natural radius of the needle that can be achieved via alternating insertions and 180° rotations of the needle shaft. In effect, the low-level 2D plane-following controller designed by Kallem *et al.*, described below, ensures that the needle remains close to a desired 2D plane, on top of which Alterovitz *et al.*'s planner can operate.

Kallem and Cowan [37, 38] developed a feedback-based estimator-controller pair to drive the needle to a desired plane, and subsequently generalized this to other subspace trackers [36]. The feedback signal used is the needle-tip position. For this task, they showed that considering a three-state system is sufficient, which simplified the estimation and control design needed to achieve the task. This controller has been successfully tested in simulations and in artificial tissue. Figure 10 shows successful experimental results of a needle being driven to a desired plane when inserted into artificial tissue.

Reed *et al.* [60] integrated the full 6-DOF asymptotic observer and the planar controller with the 2D planner of Alterovitz *et al.* [12] and the torsional compensator of Reed [59]. Figure 3 *Second Row, Right Column* shows the path taken by the unified system to reach a target inside the tissue. The goal is to reach the circular target while avoiding the polygon obstacles in the workspace. The planar controllers act every 1 mm of needle insertion into the tissue to drive the needle to the desired 2D

plane and the the planner acts at 1 cm insertion intervals. With integrated planning and control, the needle successfully reaches the target (as shown in the pre-curved tip example in Figure 3 [60]).

6 Conclusions

This chapter provides an overview of the technological and algorithmic state-of-the-art in needle steering. As can be seen from this chapter, numerous components are required to enable needle steering. Ultimately, the clinical success of needle steering depends on uniting these pieces and reducing them to practice in a driving application to create a fully integrated clinical needle steering system. As shown in Figure 2, such a system includes a set of computational and physical components – including the robotic device and steering mechanism, modeling, planning, imaging, and control – each of which is addressed in Sections 2–5.

A potential first driving application for needle steering is transperineal prostate brachytherapy, a treatment that involves implantation of radioactive seeds by needles into the prostate in order to kill cancer with radiation. Literature shows that reducing surgical trauma of the prostate reduces the severity of edema, thereby improving implant dosimetry and reducing toxicity. Current manual needle placement can involve multiple reinsertions and adjustments of the needle before it reaches a target, causing excessive trauma to the prostate. We hypothesize robotic needle steering will eliminate needle reinsertions and adjustments, and thus lead to reduction of surgical trauma. Efforts are underway by some of the authors of this chapter to create a clinically viable needle steering system for prostate brachytherapy. Along the way, we expect there to be continued advances in devices, models, planning, sensing, and control that will lead to advances in needle steering, as well as robotics in general.

Acknowledgements The authors thank Dr. Purang Abolmaesumi and Meysam Torabi for their detailed feedback on this chapter. This work was supported in part by the National Institutes of Health under Grants R21-EB003452, R01-EB006435, and F32-CA124138.

References

1. Abolhassani, N., Patel, R.V., Ayazi, F.: Minimization of needle deflection in robot-assisted percutaneous therapy. Int. J. Med. Robot. and Comp. Assist. Surg. **3**, 140–148 (2007)
2. Aboofazeli, M., Abolmaesumi, P., Mousavi, P., Fichtinger, G.: A new scheme for curved needle segmentation in three-dimensional ultrasound images. In: Proc. IEEE Int. Symp. on Biomedical Imaging, pp. 1067–1070. Boston, MA (2009)
3. Alterovitz, R., Branicky, M., Goldberg, K.: Constant-curvature motion planning under uncertainty with applications in image-guided medical needle steering. In: S. Akella, N.M. Amato, W.H. Huang, B. Mishra (eds.) Algorithmic Foundations of Robotics, *Springer Tracts in Advanced Robotics*, vol. 47, pp. 319–334. Springer-Verlag, Berlin, Germany (2008)

4. Alterovitz, R., Branicky, M., Goldberg, K.: Motion planning under uncertainty for image-guided medical needle steering. Int. J. Robot. Res. **27**(11-12), 1361–1374 (2008)
5. Alterovitz, R., Goldberg, K.: Motion Planning in Medicine: Optimization and Simulation Algorithms for Image-Guided Procedures, *Springer Tracts in Advanced Robotics*, vol. 50. Springer, Berlin, Germany (2008)
6. Alterovitz, R., Goldberg, K., Okamura, A.M.: Planning for steerable bevel-tip needle insertion through 2D soft tissue with obstacles. In: Proc. IEEE Int. Conf. Robot. and Autom., pp. 1652–1657. Barcelona, Spain (2005)
7. Alterovitz, R., Goldberg, K., Pouliot, J., Taschereau, R., Hsu, C.I.: Needle insertion and radioactive seed implantation in human tissues: simulation and sensitivity analysis. In: Proc. IEEE Int. Conf. Robot. and Autom., vol. 2, pp. 1793–1799. Taipei, Taiwan (2003)
8. Alterovitz, R., Goldberg, K.Y., Pouliot, J., Hsu, I.C.: Sensorless motion planning for medical needle insertion in deformable tissues. IEEE Trans. Information Technology in Biomedicine **13**(2), 217–225 (2009)
9. Alterovitz, R., Lim, A., Goldberg, K., Chirikjian, G.S., Okamura, A.M.: Steering flexible needles under markov motion uncertainty. In: Proc. IEEE/RSJ Int. Conf. on Intell. Robots and Syst., pp. 1570–1575 (2005)
10. Alterovitz, R., Pouliot, J., Taschereau, R., Hsu, I.C., Goldberg, K.: Needle insertion and radioactive seed implantation in human tissues: Simulation and sensitivity analysis. In: Proc. IEEE Int. Conf. Robot. and Autom., vol. 2, pp. 1793–1799. Taipei, Taiwan (2003)
11. Alterovitz, R., Pouliot, J., Taschereau, R., Hsu, I.C., Goldberg, K.: Simulating needle insertion and radioactive seed implantation for prostate brachytherapy. In: J.D. Westwood, H.M. Hoffman, G.T. Mogel, R. Phillips, R.A. Robb, D. Stredney (eds.) Medicine Meets Virtual Reality, pp. 19–25. IOS Press, Newport Beach, CA (2003)
12. Alterovitz, R., Siméon, T., Goldberg, K.: The Stochastic Motion Roadmap: A sampling framework for planning with Markov motion uncertainty. In: W. Burgard, O. Brock, C. Stachniss (eds.) Proc. Robotics: Science and Systems, pp. 246–253. MIT Press, Cambridge, MA (2008)
13. Bogdanich, W.: At V.A. hospital, a rogue cancer unit. The New York Times (2009)
14. Chentanez, N., Alterovitz, R., Ritchie, D., Cho, L., Hauser, K.K., Goldberg, K., Shewchuk, J.R., O'Brien, J.F.: Interactive simulation of surgical needle insertion and steering. In: Proc. of ACM SIGGRAPH, pp. 1–10 (2009)
15. Cheung, S., Rohling, R.: Enhancement of needle visibility in ultrasound-guided percutaneous procedures. Ultrasound Med. Biol. **30**(5), 617–624 (2004)
16. Crouch, J.R., Schneider, C.M., Wainer, J., Okamura, A.M.: A velocity-dependent model for needle insertion in soft tissue. In: Medical Image Computing and Computer Assisted Intervention, *Lecture Notes in Computer Science*, vol. 3750, pp. 624–632. Springer, Berlin/Heidelberg (2005)
17. DiMaio, S.P., Kacher, D.F., Ellis, R.E., Fichtinger, G., Hata, N., Zientara, G.P., Panych, L.P., Kikinis, R., Jolesz, F.A.: Needle artifact localization in 3T MR images. Stud. Health Technol. Inform. **119**, 120–125 (2006)
18. DiMaio, S.P., Salcudean, S.E.: Needle insertion modeling and simulation. IEEE Trans. Robot. and Autom. **19**(5), 864–875 (2003)
19. DiMaio, S.P., Salcudean, S.E.: Needle steering and motion planning in soft tissues. IEEE Trans. Biomed. Eng. **52**(6), 965–974 (2005)
20. Ding, M., Fenster, A.: A real-time biopsy needle segmentation technique using hough transform. Med Phys **30**(8), 2222–2233 (2003)
21. Ding, M., Fenster, A.: Projection-based needle segmentation in 3D ultrasound images. Comput. Aided Surg. **9**(5), 193–201 (2004)
22. Duindam, V., Alterovitz, R., Sastry, S., Goldberg, K.: Screw-based motion planning for bevel-tip flexible needles in 3D environments with obstacles. In: Proc. IEEE Int. Conf. Robot. and Autom., pp. 2483–2488 (2008)
23. Duindam, V., Xu, J., Alterovitz, R., Sastry, S., Goldberg, K.: 3D motion planning algorithms for steerable needles using inverse kinematics. In: G.S. Chirikjian, H. Choset, M. Morales, T. Murphey (eds.) Algorithmic Foundations of Robotics VIII, Springer Tracts in Advanced Robotics, pp. 535–550. Springer-Verlag, Berlin (2010)

24. Dupont, P.E., Lock, J.L., Itkowitz, B., Butler, E.: Design and control of concentric-tube robots. IEEE Trans. Robot. **26**(2), 209–225 (2010)
25. Ebert-Uphoff, I., Chirikjian, G.S.: Inverse kinematics of discretely actuated hyper-redundant manipulators using workspace densities. In: Proc. IEEE Int. Conf. Robot. and Autom., pp. 139–145 (1996)
26. Engh, J., Podnar, G., Kondziolka, D., Riviere, C.: Toward effective needle steering in brain tissue. In: Proc. IEEE Int. Conf. Eng. Med. Biol. Soc., pp. 559–562 (2006)
27. Fichtinger, G., Fiene, J., Kennedy, C.W., Kronreif, G., Iordachita, I., Song, D.Y., Burdette, E.C., Kazanzides, P.: Robotic assistance for ultrasound guided prostate brachytherapy. In: Medical Image Computing and Computer Assisted Intervention, Lecture Notes in Computer Science, pp. 119–127. Springer, Brisbane, Australia (2007)
28. Glozman, D., Shoham, M.: Image-guided robotic flexible needle steering. IEEE Trans. Robot. **23**(3), 459–467 (2007)
29. Harmat, A., Rohling, R.N., Salcudean, S.E.: Needle tip localization using stylet vibration. Ultrasound Med. Biol. **32**(9), 1339–1348 (2006)
30. Hauser, K., Alterovitz, R., Chentanez, N., Okamura, A., Goldberg, K.: Feedback control for steering needles through 3D deformable tissue using helical paths. In: Proc. Robotics: Science and Systems. Seattle, USA (2009)
31. Heverly, M., Dupont, P., Triedman, J.: Trajectory optimization for dynamic needle insertion. In: Proc. IEEE Int. Conf. Robot. and Autom., vol. 1, pp. 1646–1651. Barcelona, Spain (2005)
32. Hing, J.T., Brooks, A.D., Desai, J.P.: Reality-based needle insertion simulation for haptic feedback in prostate brachytherapy. In: Proc. IEEE Int. Conf. Robot. and Autom., vol. 1, pp. 619–624. Orlando, USA (2006)
33. Jain, A.K., Mustafa, T., Zhou, Y., Burdette, C., Chirikjian, G.S., Fichtinger, G.: Ftrac–a robust fluoroscope tracking fiducial. Med. Phys. **32**(10), 3185–3198 (2005)
34. Kallem, V.: Vision-based control on lie groups with application to needle steering. Ph.D. thesis, Johns Hopkins University (2008)
35. Kallem, V., Chang, D.E., Cowan, N.J.: Task-induced symmetry and reduction in kinematic systems with application to needle steering. In: Proc. IEEE/RSJ Int. Conf. on Intell. Robots and Syst., pp. 3302–3308. San Diego, CA (2007)
36. Kallem, V., Chang, D.E., Cowan, N.J.: Task-induced symmetry and reduction with application to needle steering. IEEE Trans. Autom. Control **55**(3), 664–673 (2010)
37. Kallem, V., Cowan, N.J.: Image-guided control of flexible bevel-tip needles. In: Proc. IEEE Int. Conf. Robot. and Autom., pp. 3015–3020. Rome, Italy (2007)
38. Kallem, V., Cowan, N.J.: Image guidance of flexible tip-steerable needles. IEEE Trans. Robot. **25**, 191–196 (2009)
39. Krieger, A., Susil, R.C., Ménard, C., Coleman, J.A., Fichtinger, G., Atalar, E., Whitcomb, L.L.: Design of a novel MRI compatible manipulator for image guided prostate interventions. IEEE Trans. Biomed. Eng. **52**(2), 306–313 (2005)
40. Mallapragada, V.G., Sarkar, N., Podder, T.K.: Robot-assisted real-time tumor manipulation for breast biopsy. IEEE Trans. Robot. **25**(2), 316–324 (2009)
41. Mason, R., Burdick, J.: Trajectory planning using reachable-state density functions. In: Proc. IEEE Int. Conf. Robot. and Autom., pp. 273–280 (2002)
42. Minhas, D.S., Engh, J.A., Fenske, M.M., Riviere, C.N.: Modeling of needle steering via duty-cycled spinning. Proc. IEEE Int. Conf. Eng. Med. Biol. Soc. **2007**, 2756–2759 (2007)
43. Misra, S., Ramesh, K.T., Okamura, A.M.: Modeling of tool-tissue interactions for computer-based surgical simulation: A literature review. Presence: Teleoperators & Virtual Environments **17**(5), 463–491 (2008)
44. Misra, S., Reed, K.B., Douglas, A.S., Ramesh, K.T., Okamura, A.M.: Needle-tissue interaction forces for bevel-tip steerable needles. In: Proc. IEEE/RASJ Int. Conf. on Biomed. Robotics and Biomechatronics, pp. 224–231. Scottsdale, USA (2008)
45. Misra, S., Reed, K.B., Ramesh, K.T., Okamura, A.M.: Observations of needle-tissue interactions. In: Proc. IEEE Int. Conf. Eng. Med. Biol. Soc., pp. 262–265. Minneapolis, USA (2009)

46. Misra, S., Reed, K.B., Schafer, B.W., Ramesh, K.T., Okamura, A.M.: Observations and models for needle-tissue interactions. In: Proc. IEEE Int. Conf. Robot. and Autom., pp. 2687–2692. Kobe, Japan (2009)
47. Misra, S., Reed, K.B., Schafer, B.W., Ramesh, K.T., Okamura, A.M.: Mechanics of flexible needles robotically steered through soft tissue. Int. J. Robot. Res. (2010). In press
48. Mozer, P.C., Partin, A.W., Stoianovici, D.: Robotic image-guided needle interventions of the prostate. Rev. Urol. **11**(1), 7–15 (2009)
49. Nienhuys, H.W., van der Stappen, F.A.: A computational technique for interactive needle insertions in 3D nonlinear material. In: Proc. IEEE Int. Conf. Robot. and Autom., vol. 2, pp. 2061–2067. New Orleans, USA (2004)
50. Novotny, P.M., Stoll, J.A., Vasilyev, N.V., del Nido, P.J., Dupont, P.E., Zickler, T.E., Howe, R.D.: GPU based real-time instrument tracking with three-dimensional ultrasound. Med. Image Anal. **11**(5), 458–464 (2007)
51. Okamura, A.M., Simone, C., O'Leary, M.D.: Force modeling for needle insertion into soft tissue. IEEE Trans. Biomed. Eng. **51**(10), 1707–1716 (2004)
52. Okazawa, S., Ebrahimi, R., Chuang, J., Salcudean, S.E., Rohling, R.: Hand-held steerable needle device. IEEE/ASME Trans. Mechatronics **10**(3), 285–296 (2005)
53. Okazawa, S.H., Ebrahimi, R., Chuang, J., Rohling, R.N., Salcudean, S.E.: Methods for segmenting curved needles in ultrasound images. Med Image Anal **10**(3), 330–342 (2006)
54. Park, W., Kim, J.S., Zhou, Y., Cowan, N.J., Okamura, A.M., Chirikjian, G.S.: Diffusion-based motion planning for a nonholonomic flexible needle model. In: Proc. IEEE Int. Conf. Robot. and Autom., pp. 4600–4605. Barcelona, Spain (2005)
55. Park, W., Liu, Y., Zhou, Y., Moses, M., Chirikjian, G.S.: Kinematic state estimation and motion planning for stochastic nonholonomic systems using the exponential map. Robotica **26**, 419–434 (2008)
56. Park, W., Wang, Y., Chirikjian, G.S.: The path-of-probability algorithm for steering and feedback control of flexible needles. Int. J. Robot. Res. **29**(7), 813830 (2010)
57. Park, W., Wang, Y., Chirikjian, G.S.: Path planning for flexible needles using second order error propagation. In: G.S. Chirikjian, H. Choset, M. Morales, T. Murphey (eds.) Algorithmic Foundations of Robotics VIII, Springer Tracts in Advanced Robotics, pp. 583–598. Springer-Verlag, Berlin (2010)
58. Podder, T., Clark, D., Sherman, J., Fuller, D., Messing, E., Rubens, D., Strang, J., Liao, L., Ng, W.S., Yu, Y.: In vivo motion and force measurement of surgical needle intervention during prostate brachytherapy. Med. Phys **33**(8), 2915–2922 (2006)
59. Reed, K.B.: Compensating for torsion windup in steerable needles. In: Proc. IEEE/RASJ Int. Conf. on Biomed. Robotics and Biomechatronics, pp. 936–941. Scottsdale, AR, USA (2008)
60. Reed, K.B., Kallem, V., Alterovitz, R., Goldberg, K., Okamura, A.M., Cowan, N.J.: Integrated planning and image-guided control for planar needle-steering. In: Proc. IEEE/RASJ Int. Conf. on Biomed. Robotics and Biomechatronics, pp. 819–824. Scottsdale, AR, USA (2008)
61. Reed, K.B., Okamura, A.M., Cowan, N.J.: Modeling and control of needles with torsional friction. IEEE Trans. Biomed. Eng. **56**(12), 2905–2916 (2009)
62. Rucker, D.C., Webster III, R.J., Chirikjian, G.S., Cowan, N.J.: Equilibrium conformations of concentric-tube continuum robots. Int. J. Robot. Res. (2010). In press (published online April 1, 2010)
63. Sears, P., Dupont, P.: A steerable needle technology using curved concentric tubes. In: Proc. IEEE/RSJ Int. Conf. on Intell. Robots and Syst., pp. 2850–2856 (2006)
64. Sitzman, B.T., Uncles, D.R.: The effects of needle type, gauge, and tip bend on spinal needle deflection. Anesth. Analg. **82**(2), 297–301 (1996)
65. Susil, R.C., Ménard, C., Krieger, A., Coleman, J.A., Camphausen, K., Choyke, P., Fichtinger, G., Whitcomb, L.L., Coleman, C.N., Atalar, E.: Transrectal prostate biopsy and fiducial marker placement in a standard 1.5T magnetic resonance imaging scanner. J. Urol. **175**(1), 113–120 (2006)
66. Taschereau, R., Pouliot, J., Roy, J., Tremblay, D.: Seed misplacement and stabilizing needles in transperineal permanent prostate implants. Radiotherapy and Oncology **55**(1), 59–63 (2000)

67. Torabi, M., Hauser, K., Alterovitz, R., Duindam, V., Goldberg, K.: Guiding medical needles using single-point tissue manipulation. In: Proc. IEEE Int. Conf. Robot. and Autom., pp. 2705–2710. Kobe, Japan (2009)
68. Wang, Y., Chirikjian, G.S.: Error propagation on the Euclidean group with applications to manipulator kinematics. IEEE Trans. Robot. **22**(4), 591–602 (2006)
69. Wang, Y., Chirikjian, G.S.: Nonparametric second-order theory of error propagation on motion groups. Int. J. Robot. Res. **27**, 1258–1273 (2008)
70. Webster III, R.J., Kim, J.S., Cowan, N.J., Chirikjian, G.S., Okamura, A.M.: Nonholonomic modeling of needle steering. Int. J. Robot. Res. **25**(5–6), 509–525 (2006)
71. Webster III, R.J., Memisevic, J., Okamura, A.M.: Design considerations for robotic needle steering. In: Proc. IEEE Int. Conf. Robot. and Autom., vol. 1, pp. 3588–3594. Barcelona, Spain (2005)
72. Webster III, R.J., Romano, J.M., Cowan, N.J.: Mechanics of precurved-tube continuum robots. IEEE Trans. Robot. **25**, 67–78 (2009)
73. Wedlick, T., Okamura, A.: Characterization of pre-curved needles for steering in tissue. In: Proc. IEEE Int. Conf. Eng. Med. Biol. Soc., pp. 1200–1203 (2009)
74. Xu, J., Duindam, V., Alterovitz, R., Goldberg, K.: Motion planning for steerable needles in 3D environments with obstacles using rapidly-exploring random trees and backchaining. In: Proc. IEEE Int. Conf. Automation Sci. and Eng., pp. 41–46 (2008)
75. Yan, K.G., Ng, W.S., Ling, K.V., Yu, Y., Podder, T.: High frequency translational oscillation and rotational drilling of the needle in reducing target movement. In: IEEE Int. Symp. Comp. Intell. in Robot. and Autom., pp. 163–168 (2005)